NIH Public Access
Author Manuscript
Neuron. Author manuscript; available in PMC 2013 April 26.

Published in final edited form as:
Neuron. 2012 April 26; 74(2): 331–343. doi:10.1016/j.neuron.2012.02.025.

Dynactin Is Required for Transport Initiation from the Distal Axon

Armen J. Moughamian[1] and **Erika L.F. Holzbaur**[1,2]

[1]Department of Physiology, Perelman School of Medicine at the University of Pennsylvania, D400 Richards Building, 3700 Hamilton Walk, Philadelphia, Pennsylvania 19104-6085, USA

SUMMARY

Dynactin is a required cofactor for the minus-end directed microtubule motor cytoplasmic dynein. Mutations within the highly conserved CAP-Gly domain of dynactin cause neurodegenerative disease. Here, we show that the CAP-Gly domain is necessary to enrich dynactin at the distal end of primary neurons. While the CAP-Gly domain is not required for sustained transport along the axon, we find that the distal accumulation facilitates the efficient initiation of retrograde vesicular transport from the neurite tip. Neurodegenerative disease mutations in the CAP-Gly domain prevent the distal enrichment of dynactin thereby inhibiting the initiation of retrograde transport. Thus, we propose a model in which distal dynactin is a key mediator in promoting the interaction between the microtubule, dynein motor and cargo for the efficient initiation of transport. Mutations in the CAP-Gly domain disrupt the formation of the motor-cargo complex, highlighting the specific defects in axonal transport that may lead to neurodegeneration.

Keywords

Dynactin; cytoplasmic dynein; CAP-Gly; p150^{Glued}; axonal transport; Perry syndrome; Hereditary Motor Neuropathy 7B; distal Spinal and Bulbar Muscular Atrophy

INTRODUCTION

The dynein-dynactin co-complex is the major minus-end directed microtubule (MT) motor for vesicle transport in eukaryotic cells. While the dynein motor alone is capable of producing force *in vitro*, the dynactin complex is a necessary cofactor for motor function in ce lls (Schroer, 2004). How dynactin contributes to dynein function remains unclear. The p150^{Glued} subunit of dynactin interacts directly with the dynein motor (Karki and Holzbaur, 1995; Vaughan and Vallee, 1995) and also independently binds MTs and MT plus-end binding proteins, including EB1 and EB3, via interactions mediated by the N-terminal cytoskeleton-associated protein glycine-rich (CAP-Gly) domain (Akhmanova and Steinmetz, 2008; Ligon et al., 2003; Waterman-Storer et al., 1995). These observations led to the hypothesis that the direct binding of dynactin to the MT enhances the processivity of dynein during transport (Waterman-Storer et al., 1995). This hypothesis is supported by *in*

© 2012 Elsevier Inc. All rights reserved

[2]Correspondence should be addressed to E.L.F.H (holzbaur@mail.med.upenn.edu).

Publisher's Disclaimer: This is a PDF file of an unedited manuscript that has been accepted for publication. As a service to our customers we are providing this early version of the manuscript. The manuscript will undergo copyediting, typesetting, and review of the resulting proof before it is published in its final citable form. Please note that during the production process errors may be discovered which could affect the content, and all legal disclaimers that apply to the journal pertain.

NIH-PA Author Manuscript
NIH-PA Author Manuscript
NIH-PA Author Manuscript

NIH-PA Author Manuscript

NIH-PA Author Manuscript

NIH-PA Author Manuscript

vitro biophysical studies showing that dynactin increases run lengths and enhances processivity at the single motor level (King and Schroer, 2000; Ross et al., 2006).

However, recent studies in non-neuronal cells show that the CAP-Gly domain of $p150^{Glued}$ is not necessary for normal dynein-mediated transport and localization of organelles including peroxisomes, lysosomes, and Golgi in either HeLa or S2 cells (Dixit et al., 2008; Kim et al., 2007). In yeast as well, the CAP-Gly domain of dynactin is not required for processive motility by dynein (Kardon et al., 2009), but does promote dynein-dependent nuclear movement leading to the hypothesis that the CAP-Gly domain may be necessary only when dynein needs to generate or sustain high force (Moore et al., 2009). Overall, these studies suggest that the highly conserved CAP-Gly domain in dynactin might be fully dispensable for vesicular transport in the cell.

Strikingly, however, genetic evidence reveals that the CAP-Gly domain of $p150^{Glued}$ is essential for normal neuronal function since point mutations within this domain cause two autosomal dominant human neurodegenerative disorders: Perry syndrome and distal Hereditary Motor Neuropathy 7B (HMN7B; also known as distal Spinal and Bulbar Muscular Atrophy) (Farrer et al., 2009; Puls et al., 2003). HMN7B is caused by a glycine to serine substitution at residue 59 (G59S), while Perry syndrome is caused by one of five point mutations at residues 71, 72 or 74 (G71R, G71E, G71A, T72P, Q74P) (Figures 1A and 1A′; Movie S1). The neuronal populations that degenerate in these two diseases are wholly distinct. HMN7B affects motor neurons, while Perry syndrome primarily affects dopaminergic neurons in the substantia nigra (Puls et al., 2005; Wider and Wszolek, 2008). It remains entirely unclear how these mutations, only 12–15 amino acids apart, differentially disrupt CAP-Gly domain function causing two disparate diseases.

Here, we report a specific function for the CAP-Gly domain of dynactin in neurons. Our data show that the CAP-Gly domain enhances the distal enrichment of dynactin in the neuron, leading to efficient flux of cargo from the distal neurite. This function is separable from the role of dynactin in promoting bidirectional transport along the axon. Further, we show that the known disease-associated mutations all affect CAP-Gly function, but differentially affect dynein-mediated transport along the axon, leading to a potential mechanistic explanation for the differential cell-type specific degeneration observed in HMN7B and Perry syndrome. Together, these studies establish a role for the highly conserved CAP-Gly domain of dynactin in the efficient initiation of transport in highly polarized cells. These findings therefore provide insight into both the regulation of axonal transport in the neuron and the cellular basis for the neuronal specificity of mutations in dynactin.

RESULTS

$p150^{Glued}$, but not the CAP-Gly domain, is necessary for transport along the axon

Multiple splice forms of $p150^{Glued}$ are expressed in brain, including a neuronally-enriched p135 isoform that lacks the CAP-Gly domain (Tokito et al., 1996). We asked which $p150^{Glued}$ isoforms are recruited to cargos actively transported through the cell. Quantitative analysis of the $p150^{Glued}$ isoforms that co-purified with LAMP1-enriched lysosomal fractions indicated that the full-length polypeptide is preferentially enriched in this fraction (Figures 1B and 1C). As dynein drives the motility of lysosomes along axons (Hendricks et al., 2010), the enrichment of full-length $p150^{Glued}$ that we observe suggests that the CAP-Gly domain may serve a specific function in the active transport of these vesicles.

To directly test this hypothesis, we examined the transport of lysosomes in primary dorsal root ganglion (DRG) neurons. We used siRNAs to deplete endogenous $p150^{Glued}$, and

NIH-PA Author Manuscript

NIH-PA Author Manuscript

NIH-PA Author Manuscript

achieved 60% knockdown as compared to neurons treated with scrambled control siRNAs (Figures S1A–S1C). Depletion of p150^{Glued} did not significantly disrupt neurite outgrowth, similar to knockdown of dynein (He et al., 2005), likely due to the gradual loss of the target proteins. We used LAMP1-RFP to monitor lysosome dynamics in DRG processes, which have a uniform MT polarity with plus-ends oriented distally as assessed by EB3 imaging (Figure S1D). Quantitative analysis indicated that the motility of LAMP1-RFP-labeled organelles was not different from that of organelles labeled with LysoTracker (data not shown).

Depletion of p150^{Glued} resulted in a significant decrease in the motility of both anterograde and retrograde cargos, with a corresponding increase in the non-motile fraction compared to scrambled siRNA-treated neurons (Figures 1D and 1E). These data show that the p150^{Glued} subunit of the dynein-dynactin complex is necessary for the bidirectional motility of lysosomes along the axon, consistent with previous studies demonstrating the reciprocal dependence of dynein and kinesin motors (Hendricks et al., 2010; Martin et al., 1999; Waterman-Storer et al., 1997).

Next we asked if expression of p150^{Glued} lacking the CAP-Gly domain, ⊗CAP-Gly, could rescue the arrest in motility caused by the knockdown of endogenous p150^{Glued}, as compared to rescue with the full-length protein. We used a bicistronic vector to simultaneously and independently express both siRNA-resistant p150^{Glued} and GFP, a transfection marker. Expression of either wild-type or ⊗CAP-Gly p150^{Glued} fully rescued the disruption in motility caused by the knockdown of p150^{Glued}. No significant differences in the fraction of anterograde, retrograde or non-motile events were observed among the scrambled control, wild-type and ⊗CAP-Gly rescue experiments (Figures 1D and 1E; Movie S2).

Analysis of individual tracks from the kymographs showed no difference in mean instantaneous velocities in either the anterograde or retrograde direction between wild-type and ⊗CAP-Gly expressing neurons, nor did we observe a significant difference in the number of pauses per track or the number of motility switches per track (Figures S1E–S1G). Additionally, we observed no change in the total number, apparent size or distribution of the lysosomes in the axon. Together our data demonstrate that while dynactin is required, the CAP-Gly domain of p150^{Glued} is not necessary for processive motility along the axon in primary neurons.

The CAP-Gly domain enriches dynactin at distal neurite tips

Since the CAP-Gly domain of p150^{Glued} does not contribute to the processive motility of cargos along the axon, we investigated other possible functions of the domain. In fungi, dynein and dynactin are enriched at hyphal tips (Lenz et al., 2006). We therefore hypothesized that dynein and dynactin may be similarly enriched at the ends of mammalian neurons and that this enrichment is dependent on the CAP-Gly domain.

Neurons were transfected with GFP, a marker for cytoplasmic volume, and stained for endogenous dynactin and dynein. In the distal neurite we observed a striking enrichment of dynactin but not of dynein, as compared to soluble GFP (Figure 2A). We saw a similar distal enrichment of dynactin in primary cortical, motor, and dopaminergic neurons, suggesting that this is a generally conserved mechanism (Figure S2). Line-scan analysis of the DRG neurons showed that dynactin accumulates in the distal neurite significantly more than dynein (Figure 2B). These data suggest that dynactin is specifically recruited and/or retained in the distal neurite.

NIH-PA Author Manuscript

NIH-PA Author Manuscript

NIH-PA Author Manuscript

Next we asked whether the CAP-Gly domain is necessary for this distal enrichment of dynactin. We over-expressed wild type or ⊗CAP-Gly p150^{Glued} in primary DRG neurons using a bicistronic vector that also expresses GFP. Wild-type p150^{Glued} was clearly enriched at the neurite tip, while neurons expressing ⊗CAP-Gly p150^{Glued} did not show a similar accumulation (Figure 2C). We quantified this difference using line-scan analysis and showed that wild-type p150^{Glued} is significantly enriched over the distal 10 μm of the neurite tip as compared to ⊗CAP-Gly p150^{Glued} (Figure 2D). These data demonstrate that the CAP-Gly domain functions to properly localize dynactin in the distal neurite.

Kinesin-1, but not kinesin-2, transport is necessary for the distal enrichment of dynactin

Motors from the kinesin superfamily, including kinesin-1 and kinesin-2, drive the fast axonal transport of vesicular cargos. The anterograde movement of cytosolic proteins via slow axonal transport is also dependent on kinesin-1 (Scott et al., 2011). We therefore tested whether the distal enrichment of dynactin is dependent on kinesin-1 activity by expressing either the dominant-negative kinesin-1 inhibitor, KHC-tail, or the KHC-stalk, which does not inhibit the motor and was used as a control (Konishi and Setou, 2009). We found that expression of KHC-tail disrupts the distal localization of dynactin, while expression of KHC-stalk had no effect on dynactin localization (Figure 3A). Line-scan analysis confirmed a significant difference in the distal accumulation of dynactin after expression of the KHC-tail, as compared to localization in neurons expressing either the vector and or the KHC-stalk (Figure 3B).

Kinesin-1 has not been shown to directly interact with dynactin, nor did we observe co-immunoprecipitation of the motor with p150^{Glued} expressed in COS7 cells (Figure S3). Thus the mechanism leading to kinesin-1-dependent distal localization of dynactin is likely to be indirect. In contrast, previous work has identified a direct interaction between kinesin-2 and p150^{Glued} (Deacon et al., 2003). Therefore, we tested whether kinesin-2 may also contribute to the anterograde transport of dynactin. Expression of Kif3A-HL, a dominant-negative inhibitor of kinesin-2 lacking the motor domain (Nishimura et al., 2004), did not disrupt the distal localization of dynactin observed in DRG neurons (Figure 3C). Line-scan analysis confirmed the distal enrichment of dynactin in neurons expressing Kif3A-HL (Figure 3D). Together, these observations indicate that kinesin-1, but not kinesin-2, mediates the anterograde delivery of dynactin to the distal neurite. This may involve either fast axonal transport as both kinesin-1 and dynactin are enriched in the same vesicular fraction (Hendricks et al., 2010), or slow axonal transport via the kinesin-1 dependent delivery of cytoplasmic cargos.

The highly stable pool of distal dynactin is retained by EBs

To understand the dynamicity of this distal pool of dynactin, we performed fluorescence recovery after photobleaching (FRAP) experiments on the distal neurite after expression of either EGFP-tagged p150^{Glued} or EGFP alone. We found that the EGFP signal robustly recovered within 20 seconds while the EGFP-p150^{Glued} has negligible recovery by 180 seconds (Figures 4A and 4B). We calculated the mobile fraction for each construct, and found that mobility of EGFP-p150^{Glued} was significantly reduced compared to EGFP (Figure 4C). These data show that the distal pool of dynactin is highly stable and suggest that dynactin is actively retained in the distal neurite.

The end-binding proteins (EBs), EB1 and EB3, are clear candidates to retain dynactin in the distal neurite. EBs are enriched on MT plus-ends, forming comet tails, and interact directly with dynactin via the CAP-Gly domain (Figure 4D). In neurons expressing mCherry-EB3 there was a significant increase in comet density in the distal neurite as compared to comet density along the axon (Figure 4E) Since the distal accumulation of dynactin is dependent

NIH-PA Author Manuscript

NIH-PA Author Manuscript

NIH-PA Author Manuscript

on the CAP-Gly domain, we hypothesized that the direct interaction of the CAP-Gly domain with the EB proteins might retain dynactin in the distal neurite.

To test this hypothesis, we depleted endogenous EBs (EB1 and EB3) using siRNA, achieving 80% knockdown of EB1 and 100% knockdown of EB3 as compared to control siRNAs (Figures 4F and 4G). Similar to the knockdown of $p150^{Glued}$, we did not observe any significant defects in neurite outgrowth or morphology after knockdown of EB1 and EB3. Staining siRNA-treated neurons for endogenous $p150^{Glued}$ demonstrated that depletion of the EBs disrupted the distal localization of dynactin as compared to control neurons (Figure 4H). Line-scan analysis revealed that knockdown of the EBs resulted in a significant difference in the localization of dynactin in the distal 7.8 μm of the axon (Figure 4I). Thus, the increased density of EBs observed in the distal axon functions to actively retain a highly stable pool of dynactin in the distal neurite via direct interaction with the CAP-Gly domain.

The CAP-Gly domain enhances flux from distal neurite tips

The function of this distal accumulation of dynactin in neurons is unknown. As full-length $p150^{Glued}$ is enriched on vesicles (Figure 1B) and the CAP-Gly domain is necessary to concentrate dynactin in the distal neurite (Figure 2C), we reasoned that the CAP-Gly domain might promote retrograde transport from the neurite tip.

We tested this hypothesis by measuring the retrograde flux of LAMP1 vesicles originating from the 10 μm zone of distally enriched dynactin. In primary DRG neurons, treated with siRNA against $p150^{Glued}$ and expressing either full-length or ⊗CAP-Gly $p150^{Glued}$, we photobleached the axon in a zone 10 μm proximal to the neurite tip to permit visualization of only those retrograde cargos that originate from the distal neurite (Figure 5A). We found that the number of vesicles leaving the distal neurite was significantly reduced (65%) in neurons expressing ⊗CAP-Gly $p150^{Glued}$, as compared to either neurons expressing wild-type $p150^{Glued}$ or untreated control neurons expressing only LAMP1-RFP (Figure 5B). Thus, the CAP-Gly domain of $p150^{Glued}$ is necessary for efficient cargo flux from the neurite tip.

Interestingly, we observed no significant accumulation or depletion (P=0.85) of LAMP1 intensity in the distal neurite after knockdown and rescue with ΔCAP-Gly $p150^{Glued}$. These data show that the decrease in flux we observed is not due to a decrease in the number of lysosomes and suggest there is likely a complex regulation of lysosome dynamics in the distal neurite. Further, we photobleached LAMP1 in the midaxon (>100 μm from the neurite end) and observed no change in the retrograde flux of lysosomes after $p150^{Glued}$ knockdown and rescue with either wild-type or ΔCAP-Gly $p150^{Glued}$ (Figure S4). These data are consistent with the axonal transport data presented in Figure 1 and show that the CAP-Gly domain of $p150^{Glued}$ is not necessary for sustained vesicular transport along the axon.

Thus, we show that the CAP-Gly domain is important for the efficient initiation of transport specifically from the distal neurite but is dispensable for transport along the axon. We propose a model in which the distally enriched dynactin acts a key mediator of the initial interaction between the MT, dynein motor and cargo to facilitate the formation of a motile motor-cargo complex and promote the efficient flux of cargos out of the distal neurite (Figure 5C).

Perry syndrome mutants disrupt CAP-Gly interactions, while the HMN7B mutant is aggregation prone and does not associate with dynein

We used the Perry syndrome and HMN7B disease mutations to test our model for the function of the CAP-Gly domain in neurons. Although the point mutations that cause these two diseases are close in primary sequence, they map to distinct regions of the three-

NIH-PA Author Manuscript

NIH-PA Author Manuscript

NIH-PA Author Manuscript

dimensional structure of the CAP-Gly domain (Figures 1A and 1A′, Movie S1). The HMN7B mutation alters a highly conserved glycine residue in the center of the globular domain. This glycine residue is important in maintaining the fold of the domain (Li et al., 2002), so mutation of this residue to a larger serine residue is predicted to decrease protein stability. In contrast, the Perry syndrome mutations are surface exposed. These residues are within or near the conserved GKNDG motif important in forming the highly conserved groove necessary for binding tubulin and EBs (Hayashi et al., 2005; Honnappa et al., 2006), so these mutations will likely disrupt these protein-protein interactions. Thus we hypothesized that the HMN7B and Perry syndrome mutations differentially disrupt CAP-Gly function due to the their location within distinct regions of the CAP-Gly domain.

Both the HMN7B (G59S) and the Perry syndrome (G71R, Q74P) mutations decrease the affinity of $p150^{Glued}$ for MTs *in vitro*, similar to the binding affinity observed with ⊗CAP-Gly $p150^{Glued}$ (Figures S5A–S5C). In assays examining over-expression of the disease-associated mutations in COS7 cells, we also observed a loss of MT binding similar to that induced by expression of ΔCAP-Gly $p150^{Glued}$ (Figures S6A and S6B). *In vitro* binding experiments also showed that the HMN7B (G59S) and Perry syndrome (G71R, Q74P) mutations significantly disrupt the interaction of $p150^{Glued}$ with EB1 (Figures S5D and S5E). Together, these results indicate that both the HMN7B and Perry syndrome mutations cause a loss of CAP-Gly function.

Interestingly however, we noted an interesting difference between the cellular phenotype of the HMN7B and Perry syndrome mutations. The Perry syndrome mutations (G71R, Q74P) predominately phenocopy the diffuse staining pattern observed upon expression of ⊗CAP-Gly $p150^{Glued}$. In contrast, the HMN7B (G59S) mutation had a greater propensity to aggregate (Figures S6A and S6B). *In vitro* studies further support this observation, as the HMN7B mutation induced the formation of $p150^{Glued}$ aggregates significantly more than either wild-type or the Perry syndrome mutants (Figures S6C and S6D). These data, along with previous observations (Levy et al., 2006), show that the HMN7B mutation decreases $p150^{Glued}$ stability while the Perry syndrome mutations do not.

We next asked if the increased aggregation of the HMN7B protein disrupts the integrity of the dynein-dynactin complex. We co-expressed myc-tagged wild-type or mutant forms of $p150^{Glued}$ along with HA-tagged wild-type $p150^{Glued}$ in COS-7 cells and performed co-immunoprecipitation assays (Figure 6). Wild-type $p150^{Glued}$ robustly co-immunoprecipitated with both the Perry syndrome (G71R and Q74P) and HMN7B (G59S) mutants (Figure 6C). These mutants also co-immunoprecipitated endogenous p50/dynamtin, another subunit of dynactin (Figure 6D). Together, these data show that both the Perry syndrome and HMN7B mutants dimerize with wild-type $p150^{Glued}$ and are incorporated into the dynactin complex.

However, we observed a striking difference in the co-immunoprecipitation of the dynein intermediate chain (DIC) between the HMN7B (G59S) and Perry syndrome (G71R, Q74P) mutants. The Perry syndrome mutants associated with DIC as strongly as wild-type $p150^{Glued}$, while the HMN7B mutant exhibited a significantly decreased association (Figure 6E). These data suggest that although the HMN7B mutation incorporates into dynactin, it does not efficiently bind to dynein. The decrease in association with dynein is likely a consequence of the altered confirmation of the HMN7B protein rather than direct perturbation the binding motif, since glycine-59 is distant from the previously identified DIC interaction region of $p150^{Glued}$ (Karki and Holzbaur, 1995; Vaughan and Vallee, 1995).

NIH-PA Author Manuscript

NIH-PA Author Manuscript

NIH-PA Author Manuscript

The HMN7B mutation disrupts transport within the axon

As a consequence of the decreased association with dynein, we hypothesized that the HMN7B mutation would disrupt axonal transport while the Perry syndrome mutations would not. To test this hypothesis we examined the transport of LAMP1-RFP in mouse primary DRG neurons expressing mutant $p150^{Glued}$.

The HMN7B (G59S) mutation caused a significant decrease in the number of retrograde and anterograde moving vesicles with a corresponding increase in the non-motile fraction (Figures 7A and 7B; Movie S5). We compared the extent of inhibition induced by the G59S mutation to the inhibition of transport caused by CC1. CC1 is a dominant-egative inhibitor of the dynein-dynactin interaction that effectively dissociates dynein and dynactin (Quintyne et al., 1999). Expression of CC1, similar to the HMN7B mutation and $p150^{Glued}$ depletion (Figure 1), caused a significant decrese in the number moving cargos and a corresponding increase in the non-motile fraction (Figures 7A and 7B; Movie S4). Immunostaining of neurons expressing the HMN7B mutant protein did not indicate the formation of frank G59S aggregates in the neuron, suggesting that the disruption in transport we observed was not due a steric inhibition of transport. Instead, these data suggest that HMN7B mutation disrupts the flux of cargos by disrupting the interaction between dynein with dynactin, similar to the effects of CC1. Importantly, these data suggest that the primary pathogenic mechanism involved in HMN7B is a disruption of axonal transport.

Analysis of individual tracks from the kymographs reveal that the HMN7B (G59S) mutation decreased the mean velocities of both anterograde and retrograde transport (Figures 7C and S7). Additionally the number of pauses per track and the number of motility switches per track were increased (Figures 7D and 7E). Together these data suggest that disruption of the dynein-dynactin interaction affects multiple parameters of dynein-mediated retrograde motility. Dominant-negative disruption decreases mean velocity and also increases the number of pauses and directional switches.

In contrast, over-expression of either Perry syndrome (G71R, Q74P) mutations or ⊗CAP-Gly $p150^{Glued}$ did not alter transport within the axon (Figure 7; Movies S4 and S5). There were no significant differences in any of the parameters of transport we measured among wild type, ΔCAP-Gly or the Perry syndrome mutations (Figures 7 and S7). At 2 DIV, we observed no significant cell death induced by expression of the mutations, nor did we observe any change in the total number or apparent size of lysosomes after expression of either the HMN7B (G59S) or Perry syndrome (G71R, Q74P) mutants. These data show that loss of CAP-Gly domain function does not have a dominant effect on transport along the axon and that the primary defect in Perry syndrome, unlike HMN7B, is not a disruption of transport within the axon.

The Perry syndrome mutation decreases flux from neurite tips

Since the CAP-Gly domain is necessary to enrich dynactin in distal neurites through an interaction with EBs (Figures 2 and 4) and both the Perry syndrome and HMN7B mutations inhibit the binding of $p150^{Glued}$ to EBs (Figure S5), we asked whether the disease-associated mutations alter the accumulation of $p150^{Glued}$ in distal neurites. Neither the Perry syndrome (G71R, Q74P) nor HMN7B (G59S) mutations showed any distal enrichment at the neurite tip compared to expression of wild-type $p150^{Glued}$ (Figures 8A and 8B). Significant differences in the accumulation of wild-type $p150^{Glued}$ compared to the Perry syndrome and HMN7B mutations occur over the first 14 μm from the neurite tip; however, expression of the mutants did not alter neurite morphology. These data further support the conclusion that both the Perry syndrome and HMN7B mutations disrupt CAP-Gly function. For the HMN7B mutation, however, it is unclear if the decreased distal accumulation is caused by a

NIH-PA Author Manuscript

NIH-PA Author Manuscript

NIH-PA Author Manuscript

decreased affinity for EBs, or is due to bidirectional inhibition of transport caused by expression of this protein, as anterograde transport is also required to establish the distal dynactin pool (Figure 3).

The accumulation of distal dynactin increases the efficient initiation of transport from the distal neurite (Figure 5). Therefore, the decreased distal accumulation caused by expression of the Perry syndrome mutations suggests that this will in turn cause decreased cargo efflux from the neurite tip. We tested this by photobleaching a region 10 μm proximal to the end of the neurite and observed the retrograde flux into the photobleached zone (Figure 8C). Expression of the G71R Perry syndrome mutation had a dominant-negative effect and significantly disrupted retrograde flux, as compared to over-expression of wild-type $p150^{Glued}$ (Figure 8D). These data suggest that the primary pathogenic mechanism in Perry syndrome is a decrease in the efficiency of retrograde transport from the distal axon (Figure 8E).

DISCUSSION

We have demonstrated a required function of the conserved CAP-Gly domain of dynactin in facilitating the efficient initiation of transport from the distal axon. We show that the CAP-Gly domain of $p150^{Glued}$ is necessary to enrich dynactin in distal neurites and that this enrichment promotes the flux of cargo out of the neurite tip. Kinesin-1 delivers dynactin to the distal neurite, while EBs retain dynactin distally and may also promote the initiation of transport by recruiting dynactin onto the MT plus-end. Once transport is initiated, the CAP-Gly domain is not necessary for transport of cargo along the axon.

The identification of the CAP-Gly motif of dynactin as an independent MT-binding domain initially suggested that it might act to enhance the processivity of the dynein motor (Hendricks et al., 2010; King and Schroer, 2000; Ross et al., 2006; Waterman-Storer et al., 1995). However, studies in S2 and HeLa cells as well as yeast show that the domain is dispensable for most interphase dynein-mediated activity in small and/or nonpolarized cells (Dixit et al., 2008; Kardon et al., 2009; Kim et al., 2007; Moore et al., 2009).

Here we show that while full-length $p150^{Glued}$ is enriched on vesicles, the CAP-Gly domain does not contribute to the motility of these vesicles along the axon. Rather, we propose a model in which the CAP-Gly domain serves a specialized function at the neurite tip (Figure 5C). The domain is necessary to enrich dynactin the distal neurite and promote the efficient initiation of retrograde transport. Previous studies have suggested that both $p150^{Glued}$ and the related CAP-Gly protein, CLIP-170, may be important in the capture of dynamic MTs for the initiation of minus-end directed transport (Lomakin et al., 2009; Vaughan et al., 2002).

We find that the distal accumulation of dynactin is dependent on kinesin-1-mediated transport. Dynactin may be delivered to the distal neurite via fast axonal transport, on anterograde-moving vesicles, or via slow axonal transport, which delivers cytoplasmic cargo and is also kinesin-1 dependent (Scott et al., 2011). Neither mechanism is likely to involve a direct interaction with dynactin. While dynein does interact with kinesin-1 (Ligon et al., 2004), dynein does not accumulate distally.

The pool of distally enriched dynactin is highly stable, suggesting a mechanism of active retention at the neurite tip. We show that the end-binding proteins, EB1 and EB3, are necessary to maintain this distal pool. Although the length of a single EB comet is 0.5–2 μm, enrichment of +TIP proteins in a spatially restricted domain may provide a platform for spatial organization in the cell (Akhmanova and Steinmetz, 2008). Thus the increased EB3 comet density we observe in the distal neurite leads to the preferential enrichment and

NIH-PA Author Manuscript

NIH-PA Author Manuscript

NIH-PA Author Manuscript

retention of dynactin in the distal neurite. In an interesting parallel, dynactin is observed to accumulate in the distal hyphal tip of filamentous fungi. Further, this localization is dependent on the MT plus-end binding protein, Peb1, which binds to the CAP-Gly domain (Lenz et al., 2006; Schuster et al., 2011), paralleling our observations in neurons. However, in fungi, dynein also accumulates in the hyphal tips. We did not observe the distal enrichment of dynein in neurons, suggesting there are likely key differences in the regulation of the motor in these two systems.

We propose a model in which the distal enrichment of dynactin enhances the coupling of dynein to the cargo and the MT to increase the efficient initiation of transport (Figure 5C). The CAP-Gly domain is necessary to enrich and retain dynactin distally where dynactin can directly interact with cargos such as late endosomes and lysosomes as well as dynein and MTs (Johansson et al., 2007; Karki and Holzbaur, 1995; Waterman-Storer et al., 1995). Thus, dynactin may be the key mediator in the formation of a motile motor-cargo complex. The distal enrichment of dynactin may promote the initial interaction of dynactin with the MT and cargo followed by the recruitment of the dynein motor. Dynein is the limiting step in the initiation of retrograde transport of the motor-cargo complex in our model; consistent with this interpretation we do not observe dynein enrichment in the distal neurite.

Axons are longer than any single MT, so cargos must switch MT tracks to efficiently transit along the axon. It is possible that dynactin also promotes this switching for vesicles in transit, by promoting the efficient formation of a cargo-motor-MT complex following interruption of motility along the axon caused by a gap in the MT track. However, our observations that a ΔCAP-Gly construct could fully rescue transport along the mid-axon suggests that this activity is not strongly required to maintain normal transport.

The importance of the CAP-Gly domain in dynactin to neuronal function is highlighted by the multiple disease-causing point mutations identified in this motif to date. Here, we show that the mechanisms driving the pathogenesis of HMN7B and Perry syndrome are distinct. The HMN7B mutation affects a residue important for maintaining the structure of the CAP-Gly domain so the mutation promotes misfolding and aggregation (Levy et al., 2006). This aggregation decreases the stability of the dynactin complex, preventing effective association between dynein and dynactin and ultimately disrupts axonal transport (Figure 8E). The Perry syndrome mutations, in contrast, are surface-exposed and more specifically disrupt protein-protein interactions. The Perry syndrome mutations phenocopy ⊗CAP-Gly $p150^{Glued}$ in all our assays, which suggests that the primary pathogenic mechanism in Perry syndrome is a loss of CAP-Gly function. Consistent with this, we observe a decrease in the efficiency of cargo flux from the distal neurite in Perry syndrome (Figure 8).

Our data on the HMN7B and Perry syndrome mutations are consistent with the pathology observed in patients and in available mouse models (Chevalier-Larsen et al., 2008; Lai et al., 2007; Laird et al., 2008). HMN7B patients have significant deposits of dynactin in motor neurons (Puls et al., 2005), while minimal aggregates of dynactin are observed Perry syndrome patients (Farrer et al., 2009). These data support a model in which the HMN7B mutation decreases $p150^{Glued}$ stability due to the critical location of glycine-59 for maintaining domain structure. In contrast, the Perry syndrome mutants cause a loss of function with no change in protein stability. Initial studies examining the effects of the Perry syndrome mutations on MT binding have yielded conflicting results (Ahmed et al., 2010; Farrer et al., 2009). However our data clearly show that the Perry syndrome mutations cause a loss of CAP-Gly function, resulting in a decrease in transport initiation from the distal neurite.

NIH-PA Author Manuscript

NIH-PA Author Manuscript

NIH-PA Author Manuscript

How do these distinct mechanisms result in the disease phenotypes associated with HMN7B and Perry syndrome? Defects in axonal transport have been observed in models of motor neuron disease and other neurodegenerative diseases (Perlson et al., 2009; Perlson et al., 2010). We speculate that multiple factors play a role in the selectivity of cell death. The HMN7B mutant protein is preferentially degraded *in vivo* (Lai et al., 2007), suggesting that most cells recognize the decreased stability of the protein and can effectively target the polypeptide for degradation. However, motor neurons may not effectively induce a stress response to protein misfolding (Batulan et al., 2003), leaving them vulnerable to the dominant-negative effect of the G59S mutation. In contrast, the distinct morphology of dopaminergic neurons may make these cells uniquely vulnerable to defects in the initiation of retrograde transport. The immense axonal arborizations of dopaminergic neurons (Matsuda et al., 2009) suggest that the loss-of-function effects of the Perry mutations may critically affect this cell type.

Thus, our data inform normal dynein-dynactin function as well as the selective vulnerabilities of discrete populations of neurons to specific perturbations in the cellular function of these proteins. The two distinct mechanisms we propose for the pathogenesis of HMN7B and Perry syndrome highlight the specialized function of a single domain of dynactin and provide a model for the function of the CAP-Gly domain of $p150^{Glued}$ in neurons.

EXPERIMENTAL PROCEDURES

DRG Culture and Transfections

Dorsal root ganglia (DRGs) were dissected from adult mice less than 1 year old and treated with 20 U/ml papain, followed by 2 mg/ml collagenase II and 2.4 mg/ml dispase II. Neurons were then dissociated in HBSS, supplemented with 5 mM HEPES and 10 mM D-glucose pH 7.35, and purified through a 20% Percoll gradient for 8 minutes at 1000xg. DRG neurons were transfected with either DNA, siRNAs or both using the basic neuron SCN nucleofector kit (Lonza) and then plated onto 0.01% poly-L-lysine and 20 μg/ml laminin coated coverslips or glass-bottom dishes (FluoroDish, World Precision Instruments) and grown for 2–4 days in F-12 medium supplemented with 10% heat-inactivated FBS and 100 U/ml penicillin-streptomycin. Live-cell imaging was done in Hibernate-A (Brain Bits, Springfield IL) supplemented with 2% B27 supplement (Invitrogen) and 2 mM GlutaMax (Gibco). All experiments involving animals were approved by the IACUC at the University of Pennsylvania.

Microscopy

Images of LAMP1-RFP motility (Figures 1 and 7) were acquired 366 ms per frame for 360 frames. Images were acquired in epifluorescence on an inverted Leica DMI-6000/ CTR-7000HS microscope with an Apochromat 63× 1.4 NA oil-immersion objective in a temperature-controlled chamber (37°C) with an ORCA R^2 (Hamamatsu) camera using LAS-AF (Leica) software. Fixed cells were imaged in epifluorescence, as described above. Neurons were imaged with a 1.6× magnifier.

Photobleaching of LAMP1-RFP (Figures 5A, S4 and 8C) and FRAP of EGFP or EGFP-$p150^{Glued}$ (Figure 4A) was performed in a temperature-controlled chamber (37°C) using the 561 nm or 488 nm laser, respectively, at 100% power for 25 cycles on the Ultraview Vox (PerkinElmer) spinning disk confocal system with an Ultraview Photokinesis (PerkinElmer) unit on an inverted Nikon Ti microscope with apochromat 100× 1.49 NA oil-immersion objective and a C9100-50 EM-CCD (Hamamatsu) camera controlled by Volocity (PerkinElmer) software. mCherry-EB3 was imaged using the 561 nm laser at 2 seconds per

NIH-PA Author Manuscript

NIH-PA Author Manuscript

NIH-PA Author Manuscript

frame for 5 minutes. For LAMP1-RFP photobleaching experiments, images were acquired using the 561 nm laser at 2 frames per second for 5 seconds prior to and for 120 seconds subsequent to photobleaching. For FRAP, images were acquired using the 488 nm laser at 1 frame per second for 5 seconds prior to and for 180 seconds subsequent to photobleaching. FRAP curves were fit to the single exponential equation, f(t)=A(1-e^-τt), where A is mobile fraction.

Image Analysis

Kymographs from time-lapse imaging data were made using the Multiple Kymograph plugin (submitted by J. Rietdorf and A. Seitz, European Molecular Biology Laboratory, Heidelberg, Germany) in ImageJ (NIH). All tracks from each LAMP1-RFP kymograph were classified as either anterograde, retrograde or non-motile. Cargos that moved net distances greater than 10 μm in a single direction were classified as either anterograde or retrograde. Cargos that moved less than 10 μm were classified as non-motile.

The tracks of individual lysosomes, moving greater than 10 μm, were determined in ImageJ by marking points where the slope changes and interpolating the intermediate points of the track using a linear function. The instantaneous velocities, pauses per track and motility switches per track were calculated from this data. A pause was defined as an instantaneous velocity less than 100 nm per second. A motility switch is defined as a change in the direction of motility (anterograde to retrograde or vice versa) or switch from directional motility (anterograde or retrograde) to a pause and vice versa.

Line-scan fluorescence intensity quantification was performed on raw imaging data using Metamorph. A line starting at the distal end of the neurite was drawn along the process towards the cell body and the florescence intensity was measured along the line. The fluorescence intensity of both channels was normalized to the minimum value of each line. The normalized intensities were divided by the corresponding normalized GFP intensity and plotted as a function of distance from the neurite tip.

The retrograde flux of LAMP1-RFP was measured from kymographs of the photobleached region of the axon, which were made prior to and subsequent to the photobleaching in Volocity (PerkinElmer). Vesicles originating from the distal end and moved at least 50 pixels (3.5 μm) into the photobleached zone were considered retrograde moving cargos.

Immunoprecipitation

To test for co-immunoprecipitation of dynactin, COS-7 cells were co-transfected with myc-tagged $p150^{Glued}$ isoforms and HA-tagged wild-type $p150^{Glued}$ using FuGENE 6 (Roche) for 24 hours. Cells were lysed in 100 mM PIPES, 1 mM EGTA, 2 mM $MgCl_2$, 25mM NaCl, 0.5mM DTT, 1% Triton X-100 and protease inhibitors (1mM PMSF, 1 mM Leupeptin, 0.001 mg/ml Pepstatin-A and 0.01 mg/ml TAME). To test for co-immunoprecipitation of KHC with $p150^{Glued}$, COS-7 cells were transfected with myc-tagged $p150^{Glued}$ isoforms and lysed in the above buffer except with 0.25% Triton X-100. Immunoprecipitations were performed using Protein G coupled Dynabeads (Invitrogen). Beads were washed in the above buffer without the detergent and eluates were analyzed by SDS-PAGE and western blot.

Statistical Methods

Statistics were performed in Prism (GraphPad) software. When comparing multiple data sets, statistical significance was determined by using a one-way or two-way ANOVA with a Bonferroni post test. A Student's t-test was used to determine statistical significance when comparing two data sets.

NIH-PA Author Manuscript

NIH-PA Author Manuscript

NIH-PA Author Manuscript

Supplementary Material

Refer to Web version on PubMed Central for supplementary material.

Acknowledgments

The authors acknowledge the scientific generosity of M. Farrer, I. Kaverina, K. Kaibuchi and Y. Konishi, support from NIH training grant 5T32AG000255 to A.J.M and NIH GM48661 to E.L.F.H.

REFERENCES

Ahmed S, Sun S, Siglin AE, Polenova T, Williams JC. Disease-associated mutations in the p150(Glued) subunit destabilize the CAP-gly domain. Biochemistry. 2010; 49:5083–5085. [PubMed: 20518521]

Akhmanova A, Steinmetz MO. Tracking the ends: a dynamic protein network controls the fate of microtubule tips. Nat Rev Mol Cell Biol. 2008; 9:309–322. [PubMed: 18322465]

Batulan Z, Shinder GA, Minotti S, He BP, Doroudchi MM, Nalbantoglu J, Strong MJ, Durham HD. High threshold for induction of the stress response in motor neurons is associated with failure to activate HSF1. J Neurosci. 2003; 23:5789–5798. [PubMed: 12843283]

Chevalier-Larsen ES, Wallace KE, Pennise CR, Holzbaur EL. Lysosomal proliferation and distal degeneration in motor neurons expressing the G59S mutation in the p150Glued subunit of dynactin. Hum Mol Genet. 2008; 17:1946–1955. [PubMed: 18364389]

Deacon SW, Serpinskaya AS, Vaughan PS, Lopez Fanarraga M, Vernos I, Vaughan KT, Gelfand VI. Dynactin is required for bidirectional organelle transport. J Cell Biol. 2003; 160:297–301. [PubMed: 12551954]

Dixit R, Levy JR, Tokito M, Ligon LA, Holzbaur EL. Regulation of dynactin through the differential expression of p150Glued isoforms. J Biol Chem. 2008; 283:33611–33619. [PubMed: 18812314]

Farrer MJ, Hulihan MM, Kachergus JM, Dachsel JC, Stoessl AJ, Grantier LL, Calne S, Calne DB, Lechevalier B, Chapon F, et al. DCTN1 mutations in Perry syndrome. Nat Genet. 2009; 41:163–165. [PubMed: 19136952]

Hayashi I, Wilde A, Mal TK, Ikura M. Structural basis for the activation of microtubule assembly by the EB1 and p150Glued complex. Mol Cell. 2005; 19:449–460. [PubMed: 16109370]

He Y, Francis F, Myers KA, Yu W, Black MM, Baas PW. Role of cytoplasmic dynein in the axonal transport of microtubules and neurofilaments. J Cell Biol. 2005; 168:697–703. [PubMed: 15728192]

Hendricks AG, Perlson E, Ross JL, Schroeder HW 3rd, Tokito M, Holzbaur EL. Motor Coordination via a Tug-of-War Mechanism Drives Bidirectional Vesicle Transport. Curr Biol. 2010

Honnappa S, Okhrimenko O, Jaussi R, Jawhari H, Jelesarov I, Winkler FK, Steinmetz MO. Key interaction modes of dynamic +TIP networks. Mol Cell. 2006; 23:663–671. [PubMed: 16949363]

Johansson M, Rocha N, Zwart W, Jordens I, Janssen L, Kuijl C, Olkkonen VM, Neefjes J. Activation of endosomal dynein motors by stepwise assembly of Rab7-RILP-p150Glued, ORP1L, and the receptor betalll spectrin. J Cell Biol. 2007; 176:459–471. [PubMed: 17283181]

Kardon JR, Reck-Peterson SL, Vale RD. Regulation of the processivity and intracellular localization of Saccharomyces cerevisiae dynein by dynactin. Proc Natl Acad Sci U S A. 2009; 106:5669–5674. [PubMed: 19293377]

Karki S, Holzbaur EL. Affinity chromatography demonstrates a direct binding between cytoplasmic dynein and the dynactin complex. J Biol Chem. 1995; 270:28806–28811. [PubMed: 7499404]

Kim H, Ling SC, Rogers GC, Kural C, Selvin PR, Rogers SL, Gelfand VI. Microtubule binding by dynactin is required for microtubule organization but not cargo transport. J Cell Biol. 2007; 176:641–651. [PubMed: 17325206]

King SJ, Schroer TA. Dynactin increases the processivity of the cytoplasmic dynein motor. Nat Cell Biol. 2000; 2:20–24. [PubMed: 10620802]

Konishi Y, Setou M. Tubulin tyrosination navigates the kinesin-1 motor domain to axons. Nat Neurosci. 2009; 12:559–567. [PubMed: 19377471]

NIH-PA Author Manuscript

NIH-PA Author Manuscript

NIH-PA Author Manuscript

Lai C, Lin X, Chandran J, Shim H, Yang WJ, Cai H. The G59S mutation in p150(glued) causes dysfunction of dynactin in mice. J Neurosci. 2007; 27:13982–13990. [PubMed: 18094236]

Laird FM, Farah MH, Ackerley S, Hoke A, Maragakis N, Rothstein JD, Griffin J, Price DL, Martin LJ, Wong PC. Motor neuron disease occurring in a mutant dynactin mouse model is characterized by defects in vesicular trafficking. J Neurosci. 2008; 28:1997–2005. [PubMed: 18305234]

Lenz JH, Schuchardt I, Straube A, Steinberg G. A dynein loading zone for retrograde endosome motility at microtubule plus-ends. EMBO J. 2006; 25:2275–2286. [PubMed: 16688221]

Levy JR, Sumner CJ, Caviston JP, Tokito MK, Ranganathan S, Ligon LA, Wallace KE, LaMonte BH, Harmison GG, Puls I, et al. A motor neuron disease-associated mutation in p150Glued perturbs dynactin function and induces protein aggregation. J Cell Biol. 2006; 172:733–745. [PubMed: 16505168]

Li S, Finley J, Liu ZJ, Qiu SH, Chen H, Luan CH, Carson M, Tsao J, Johnson D, Lin G, et al. Crystal structure of the cytoskeleton-associated protein glycine-rich (CAP-Gly) domain. J Biol Chem. 2002; 277:48596–48601. [PubMed: 12221106]

Ligon LA, Shelly SS, Tokito M, Holzbaur EL. The microtubule plus-end proteins EB1 and dynactin have differential effects on microtubule polymerization. Mol Biol Cell. 2003; 14:1405–1417. [PubMed: 12686597]

Ligon LA, Tokito M, Finklestein JM, Grossman FE, Holzbaur EL. A direct interaction between cytoplasmic dynein and kinesin I may coordinate motor activity. J Biol Chem. 2004; 279:19201–19208. [PubMed: 14985359]

Lomakin AJ, Semenova I, Zaliapin I, Kraikivski P, Nadezhdina E, Slepchenko BM, Akhmanova A, Rodionov V. CLIP-170-dependent capture of membrane organelles by microtubules initiates minus-end directed transport. Dev Cell. 2009; 17:323–333. [PubMed: 19758557]

Martin M, Iyadurai SJ, Gassman A, Gindhart JG Jr. Hays TS, Saxton WM. Cytoplasmic dynein, the dynactin complex, and kinesin are interdependent and essential for fast axonal transport. Mol Biol Cell. 1999; 10:3717–3728. [PubMed: 10564267]

Matsuda W, Furuta T, Nakamura KC, Hioki H, Fujiyama F, Arai R, Kaneko T. Single nigrostriatal dopaminergic neurons form widely spread and highly dense axonal arborizations in the neostriatum. J Neurosci. 2009; 29:444–453. [PubMed: 19144844]

Moore JK, Sept D, Cooper JA. Neurodegeneration mutations in dynactin impair dynein-dependent nuclear migration. Proc Natl Acad Sci U S A. 2009; 106:5147–5152. [PubMed: 19279216]

Nishimura T, Kato K, Yamaguchi T, Fukata Y, Ohno S, Kaibuchi K. Role of the PAR-3-KIF3 complex in the establishment of neuronal polarity. Nat Cell Biol. 2004; 6:328–334. [PubMed: 15048131]

Perlson E, Jeong GB, Ross JL, Dixit R, Wallace KE, Kalb RG, Holzbaur EL. A switch in retrograde signaling from survival to stress in rapid-onset neurodegeneration. J Neurosci. 2009; 29:9903–9917. [PubMed: 19657041]

Perlson E, Maday S, Fu MM, Moughamian AJ, Holzbaur EL. Retrograde axonal transport: pathways to cell death? Trends Neurosci. 2010; 33:335–344. [PubMed: 20434225]

Puls I, Jonnakuty C, LaMonte BH, Holzbaur EL, Tokito M, Mann E, Floeter MK, Bidus K, Drayna D, Oh SJ, et al. Mutant dynactin in motor neuron disease. Nat Genet. 2003; 33:455–456. [PubMed: 12627231]

Puls I, Oh SJ, Sumner CJ, Wallace KE, Floeter MK, Mann EA, Kennedy WR, Wendelschafer-Crabb G, Vortmeyer A, Powers R, et al. Distal spinal and bulbar muscular atrophy caused by dynactin mutation. Ann Neurol. 2005; 57:687–694. [PubMed: 15852399]

Quintyne NJ, Gill SR, Eckley DM, Crego CL, Compton DA, Schroer TA. Dynactin is required for microtubule anchoring at centrosomes. J Cell Biol. 1999; 147:321–334. [PubMed: 10525538]

Ross JL, Wallace K, Shuman H, Goldman YE, Holzbaur EL. Processive bidirectional motion of dynein-dynactin complexes in vitro. Nat Cell Biol. 2006; 8:562–570. [PubMed: 16715075]

Schroer TA. Dynactin. Annu Rev Cell Dev Biol. 2004; 20:759–779. [PubMed: 15473859]

Schuster M, Kilaru S, Ashwin P, Lin C, Severs NJ, Steinberg G. Controlled and stochastic retention concentrates dynein at microtubule ends to keep endosomes on track. EMBO J. 2011; 30:652–664. [PubMed: 21278707]

NIH-PA Author Manuscript

NIH-PA Author Manuscript

NIH-PA Author Manuscript

Scott DA, Das U, Tang Y, Roy S. Mechanistic logic underlying the axonal transport of cytosolic proteins. Neuron. 2011; 70:441–454. [PubMed: 21555071]

Tokito MK, Howland DS, Lee VM, Holzbaur EL. Functionally distinct isoforms of dynactin are expressed in human neurons. Mol Biol Cell. 1996; 7:1167–1180. [PubMed: 8856662]

Vaughan KT, Vallee RB. Cytoplasmic dynein binds dynactin through a direct interaction between the intermediate chains and p150Glued. J Cell Biol. 1995; 131:1507–1516. [PubMed: 8522607]

Vaughan PS, Miura P, Henderson M, Byrne B, Vaughan KT. A role for regulated binding of p150(Glued) to microtubule plus ends in organelle transport. J Cell Biol. 2002; 158:305–319. [PubMed: 12119357]

Waterman-Storer CM, Karki S, Holzbaur EL. The p150Glued component of the dynactin complex binds to both microtubules and the actin-related protein centractin (Arp-1). Proc Natl Acad Sci U S A. 1995; 92:1634–1638. [PubMed: 7878030]

Waterman-Storer CM, Karki SB, Kuznetsov SA, Tabb JS, Weiss DG, Langford GM, Holzbaur EL. The interaction between cytoplasmic dynein and dynactin is required for fast axonal transport. Proc Natl Acad Sci U S A. 1997; 94:12180–12185. [PubMed: 9342383]

Wider C, Wszolek ZK. Rapidly progressive familial parkinsonism with central hypoventilation, depression and weight loss (Perry syndrome)--a literature review. Parkinsonism Relat Disord. 2008; 14:1–7. [PubMed: 17870652]

NIH-PA Author Manuscript

NIH-PA Author Manuscript

NIH-PA Author Manuscript

HIGHLIGHTS

- The CAP-Gly domain is required to localize dynactin to the distal axon
- Dynactin distal localization is dependent on kinesin-1 and end-binding proteins
- Dynactin facilitates efficient transport initiation from the distal axon
- Neurodegenerative mutations disrupt distal localization and transport initiation

NIH-PA Author Manuscript

NIH-PA Author Manuscript

NIH-PA Author Manuscript

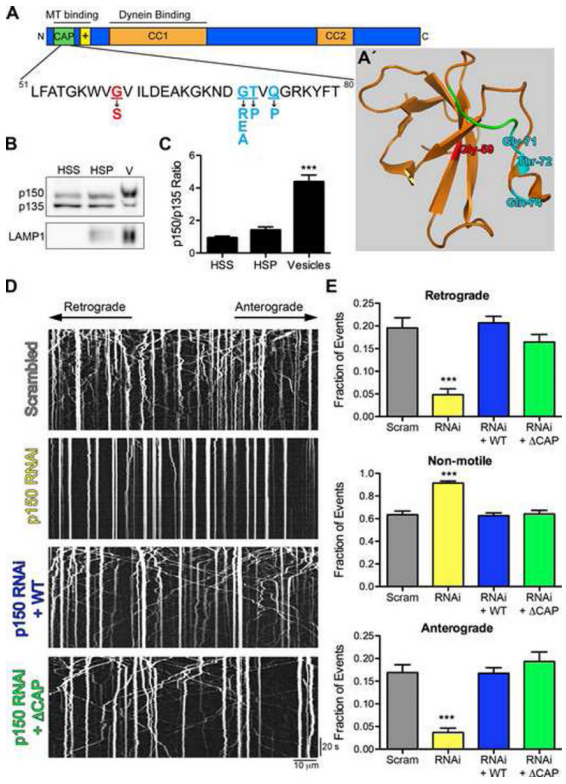

Figure 1. The highly conserved CAP-Gly domain of p150^{Glued} is not required for axonal transport of lysosomes

(A) Schematic of the p150^{Glued} subunit of dynactin. The CAP-Gly domain (green) binds both MTs and MT plus-end binding proteins. The basic domain (yellow) also independently binds MTs. The HMN7B (red) and the Perry syndrome (cyan) point mutations are shown below. (A′) Crystal structure of the CAP-Gly domain of p150^{Glued} modified from (Honnappa et al., 2006) (PDB ID 2HKQ). The GKNDG motif is in green and the disease-associated mutations are colored as in (A). The HMN7B mutation is buried at the core of the CAP-Gly domain and may disrupt protein folding, while the Perry syndrome mutations are surface-exposed and may predominantly interfere with protein-protein interactions. Also see Movie S1. (B) Purified vesicles (V) from mouse brain enriched for LAMP1 were probed for p150^{Glued} using a polyclonal antibody that recognizes both the full-length and p135 isoforms. (C) Purified vesicles had an increased ratio of full-length p150^{Glued} to p135 compared to the high speed supernatant (HSS) and high-speed pellet (HSP) fractions. Mean ± SEM, n=3 vesicle purifications, ***P<0.001 compared to HSS, one-way ANOVA Bonferroni post test. (D) Kymographs of LAMP1-RFP motility in primary dorsal root ganglion (DRG) neurons imaged at 4 days *in vitro* (DIV) after transfection with two scrambled siRNAs or two siRNAs to p150^{Glued}. siRNAs were also transfected with wild-type full-length p150^{Glued} (WT) or ΔCAP-Gly p150^{Glued} (ΔCAP) resistant to the siRNA. Kymographs drawn along neurite processes represent movement over time so motile organelles appear as diagonal lines while paused organelles appear as vertical lines. Images were acquired at 366 ms per frame for 2.2 minutes; scale bars for the x and y-axes represent 10 μm and 20 seconds, respectively. Kymographs show the first 300 frames, full movies shown in Movie S2. (E) Lysosomal motility was quantified from the kymographs. Depletion of p150^{Glued} significantly disrupted anterograde and retrograde motility and caused a corresponding increase in non-motile events. Expression of either wild-type or ⊗CAP-Gly p150^{Glued} rescued this disruption. >800 vesicles were counted per condition. Mean ± SEM,

n=12–15 neurons per condition, ***P<0.001 compared to scrambled siRNAs, one-way ANOVA Bonferroni post test. Also see Figure S1.

NIH-PA Author Manuscript
NIH-PA Author Manuscript
NIH-PA Author Manuscript

NIH-PA Author Manuscript
NIH-PA Author Manuscript
NIH-PA Author Manuscript

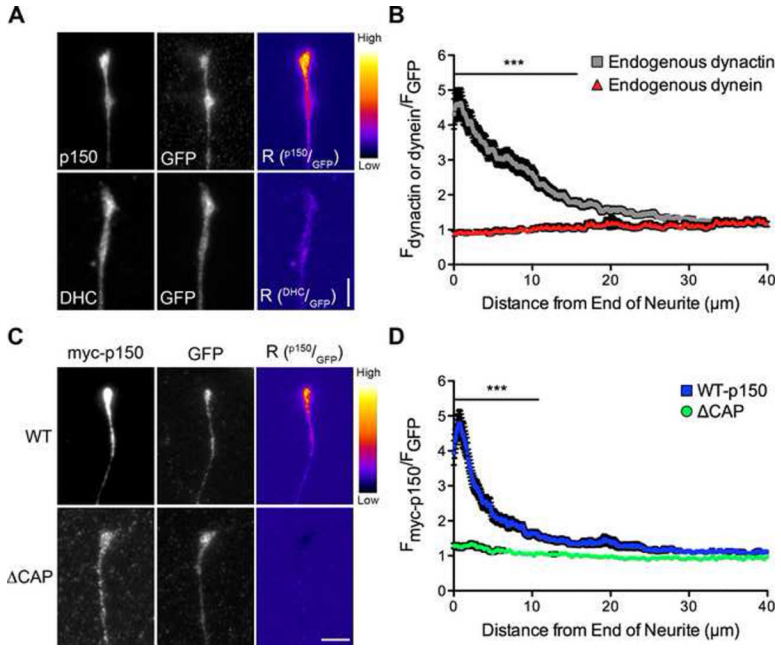

Figure 2. The CAP-Gly domain is necessary for the distal enrichment of dynactin in neurons

(A) Distal ends of DRG neurons expressing GFP were stained at 2 DIV for endogenous $p150^{Glued}$ or endogenous dynein heavy chain (DHC) and GFP, as a marker of cytoplasmic volume. These images were individually contrast enhanced to display both axonal and tip staining. The raw p150 and DHC data were divided by the corresponding raw GFP signal to create the ratio-image ($R^{p150}/_{GFP}$ or $R^{DHC}/_{GFP}$). These images show the distal accumulation relative to GFP. These ratio-images were contrast enhanced to the same level and a heat map was applied to show the relative intensities of the ratio. The warmer colors represent a higher ratio, while cooler colors represent a lower ratio. (B) Line-scan quantification of the distal accumulation. The normalized ratio of endogenous dynactin or dynein fluorescence intensity to GFP intensity was determined along the length of the neurite tip. Expression as a ratio to soluble GFP controls for changes in cytoplasmic volume. Dynactin accumulated significantly more than dynein over the distal 15 μm of the neurite. Mean ± SEM, $n \geq 41$ neurite tips from 5–7 neurons per condition, ***$P<0.001$, two-way ANOVA Bonferroni post test. (C) Images of the distal neurites of DRG neurons expressing myc-tagged full-length wild-type or ΔCAP-Gly $p150^{Glued}$ and GFP from a bicistronic vector at 2 DIV. Neurites were stained for myc and GFP and images individually contrast enhanced to display both axonal and tip staining. The corresponding ratio-images ($R^{p150}/_{GFP}$) were made from the raw imaging data and a heat map was applied as described in (A). (D) Line-scan analysis from the end of the neurite. The normalized ratio of myc-tagged $p150^{Glued}$ fluorescence intensity to GFP intensity was determined along the length of the neurite tip. Wild-type $p150^{Glued}$ accumulated significantly more over the distal 10 μm compared to ΔCAP-Gly $p150^{Glued}$. Mean ± SEM, $n \geq 29$ neurite tips from 5–6 neurons per condition, ***$P<0.001$, two-way ANOVA Bonferroni post test. Scale bars: 5 μm. Also see Figure S2.

NIH-PA Author Manuscript
NIH-PA Author Manuscript
NIH-PA Author Manuscript

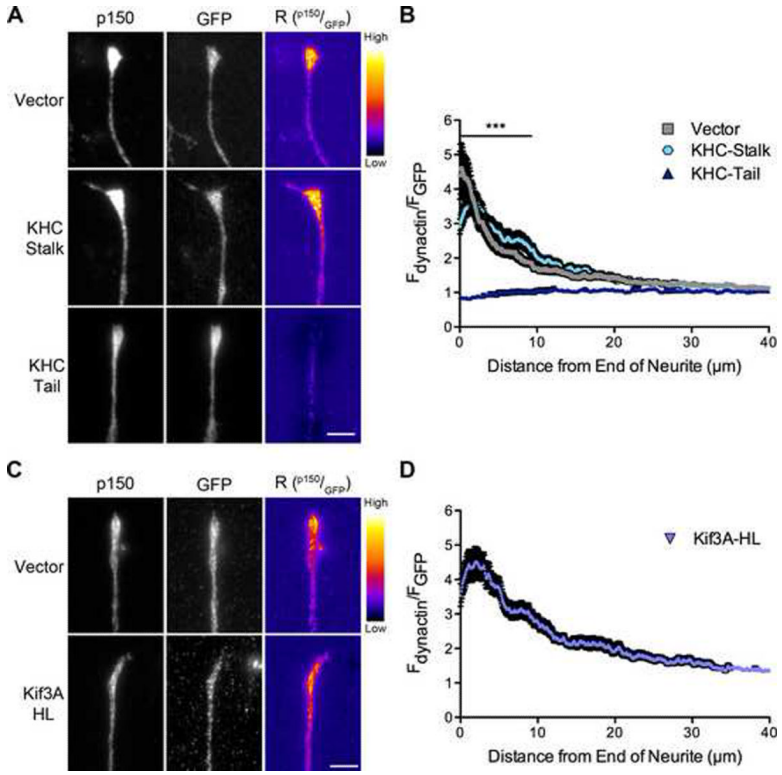

Figure 3. Kinesin-1, but not kinesin-2, contributes to the distal localization of dynactin

(A) Distal ends of DRG neurons expressing GFP, GFP-tagged KHC-stalk or GFP-tagged KHC-tail were stained at 2 DIV for endogenous $p150^{Glued}$ and GFP. These images were individually contrast enhanced to display both axonal and tip staining. The raw p150 data was divided by the corresponding raw GFP signal to create the ratio-image ($R^{p150}/_{GFP}$). These images show the distal accumulation relative to GFP. These ratio-images were contrast enhanced to the same level and a heat map was applied to show the relative intensities of the ratio. The warmer colors represent a higher ratio, while cooler colors represent a lower ratio. (B) Line-scan quantification of the distal accumulation. The normalized ratio of endogenous dynactin fluorescence intensity to GFP intensity was determined along the length of the neurite tip. The KHC-tail, a dominant-negative kinesin-1 inhibitor, significantly disrupted the localization of dynactin over the distal 9 μm of the neurite as compared to vector expressing neurons. Mean ± SEM, $n \geq 46$ neurite tips from 7–8 neurons per condition, ***$P<0.001$, two-way ANOVA Bonferroni post test. (C) Distal ends of DRG neurons expressing GFP or GFP-tagged Kif3A-HL, a dominant-negative kinesin-2 inhibitor, were stained at 2 DIV for endogenous $p150^{Glued}$ and GFP. These images were individually contrast enhanced to display both axonal and tip staining. The ratio-images ($R^{p150}/_{GFP}$) were calculated from the raw imaging data and a heat map was applied as described in (A). (D) Line-scan quantification of the distal accumulation as described in (B). Kif3A-HL expression had no effect on the distal accumulation of dynactin. Mean ± SEM, $n \geq 46$ neurite tips from 7 neurons per condition. Also see Figure S3.

NIH-PA Author Manuscript
NIH-PA Author Manuscript
NIH-PA Author Manuscript

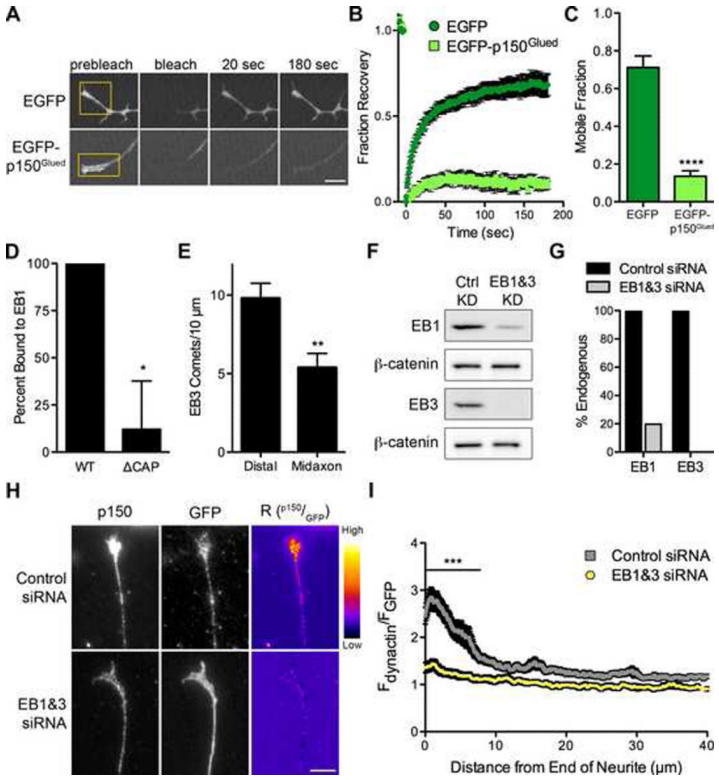

Figure 4. EBs are necessary to maintain the highly stable pool of distal dynactin

(A) FRAP time-series of the distal tip of DRG neurons at 2 DIV expressing either EGFP or EGFP-p150^{Glued}. The yellow box demarcates the photobleached region. Each image in the time-series was contrast enhanced equally. Also see Movie S3. (B) Mean FRAP recovery curve ± SEM, n=10–11 neurites per condition. Photobleaching occurred at time=0. (C) The mobile fraction for each individual FRAP trace was determined by fitting the trace to a single exponential equation. The mean mobile fraction was determined for EGFP and EGFP-p150^{Glued} expressing neurons ± SEM, n=10–11 traces per condition, ****P<0.0001, Student's t-test. (D) Quantification of EB1 binding as percent bound relative to wild-type. WT and ΔCAP p150^{Glued} fragments were synthesized *in vitro* and incubated with either EB1-conjugated or empty beads. Mean ± SEM, n=4 independent experiments, *P<0.05, Student's t-test. Also see Figure S5. (E) The number of EB3 comets was counted from time-lapse movies of DRG neurons at 2 DIV expressing mCherry-EB3. Distal neurite is defined as the distal 10 μm of the neurite while the midaxon is defined as a 10 μm region of the axon >50 μm proximal to the neurite end. Mean ± SEM, n=21 movies per condition, **P<0.01, Student's t-test. (F) Lysate from DRG neurons at 4 DIV after treatment with either control siRNAs or siRNA directed against EB1 and EB3 was probed for EB1, EB3 and β-catenin. (G) Quantification by western blot of EB1 and EB3 levels after siRNA knockdown showed approximately 80% and 100% knockdown of EB1 and EB3, respectively. Western blot values were normalized to β-catenin as a loading control. (H) Distal ends of DRG neurons at 4 DIV stained for endogenous p150^{Glued} and GFP after transfection with GFP and either control siRNAs or siRNAs against EB1 and EB3. These images were individually contrast enhanced to display both axonal and tip staining. The ratio-images ($R^{p150}/_{GFP}$) were calculated from the raw imaging data by dividing the raw p150 data by the corresponding raw GFP signal. These images show the distal accumulation relative to GFP. These ratio-images were contrast enhanced to the same level and a heat map was applied to show the relative intensities of the ratio. The warmer colors represent a higher ratio, while cooler colors represent a lower ratio. (I) Line-scan quantification of the

distal accumulation. The normalized ratio of endogenous dynactin fluorescence intensity to GFP intensity was determined along the length of the neurite tip. Expression as a ratio to soluble GFP controls for changes in cytoplasmic volume. Knockdown of EB1 and EB3 significantly reduced the distal accumulation of dynactin over 7.8 μm from the distal axon. Mean ± SEM, $n \geq 49$ neurite tips from 9–12 neurons per condition, *** $P < 0.001$, two-way ANOVA Bonferroni post test. Scale bars: 5 μm.

NIH-PA Author Manuscript
NIH-PA Author Manuscript
NIH-PA Author Manuscript

NIH-PA Author Manuscript

NIH-PA Author Manuscript

NIH-PA Author Manuscript

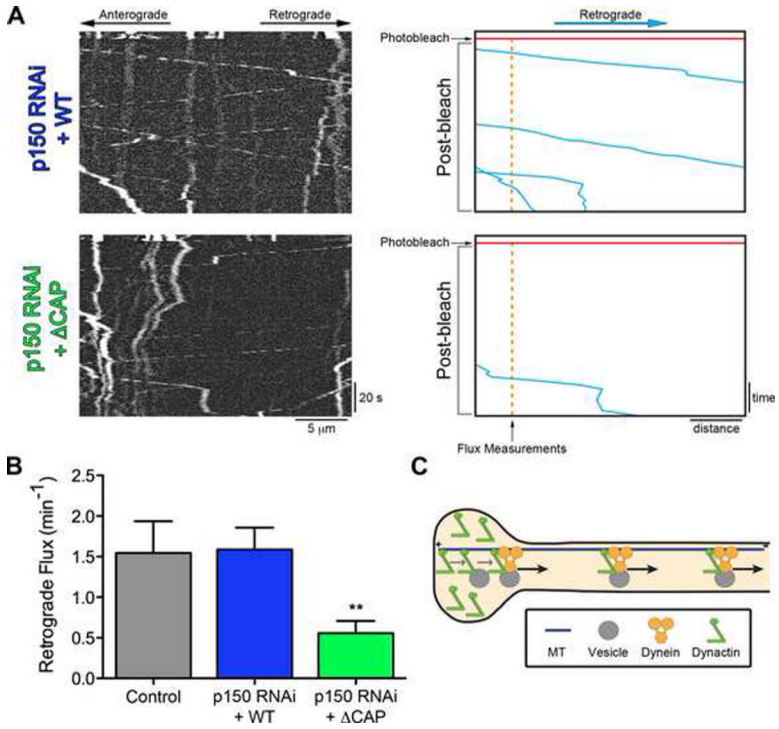

Figure 5. The CAP-Gly domain enhances the retrograde flux of cargo from the distal axon

DRG neurons were imaged at 4 DIV after transfection with siRNA to deplete endogenous p150^{Glued} and rescued with either wild-type or ΔCAP-Gly p150^{Glued}. The retrograde flux of LAMP1-RFP cargo from the end of the neurite was measured following photobleaching of a zone 10 μm proximal to the neurite end. Entry of cargos from the distal tip into this bleach zone was assessed with time-lapse imaging. Images were acquired at 2 frames per second for 5 seconds pre-photobleaching and 120 seconds post-photobleaching. (A) Kymographs of the photobleached zone were made prior to and subsequent to photobleaching to assess the retrograde flux of cargo from the distal neurite. Scale bars for the x and y-axes represent 5 μm and 20 seconds, respectively. On the right, for illustrative purposes, the retrograde moving cargos were traced over in blue, the time of photobleaching is marked in red and the point where flux measurements were made is in orange. (B) Retrograde vesicle flux was determined by counting the number of retrograde vesicles that moved at least 3.5 μm into the photobleached zone from the distal neurite. Rescue with ΔCAP-Gly p150^{Glued} significantly decreased the flux from the distal neurite as compared to either rescue with wild-type p150^{Glued} or control neurons not treated with siRNA. Mean ± SEM, n>11 neurites from 6–14 neurons per condition, ** P<0.01, compared to wild-type, one-way ANOVA Bonferroni post test. (C) Model for the function of the CAP-Gly domain of p150^{Glued} in neurons. The CAP-Gly domain is necessary to distally enrich p150^{Glued} in neurite tips and facilitate the flux of cargo from the neurite end. Also see Figure S4.

NIH-PA Author Manuscript
NIH-PA Author Manuscript
NIH-PA Author Manuscript

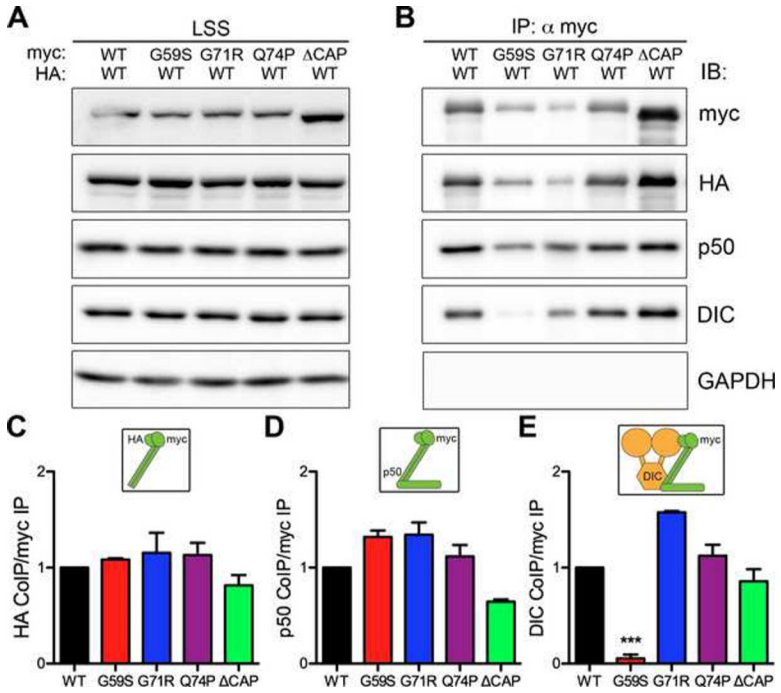

Figure 6. Decreased association of HMN7B mutant dynactin with dynein

(A) Myc-tagged wild-type (WT), HMN7B (G59S), Perry syndrome (G71R & Q74P) and ΔCAP-Gly p150^{Glued} were co-expressed with wild-type HA-tagged p150^{Glued} in COS-7 cells, LSS: low-speed supernatant. (B) Immunoprecipitation (IP) was performed using an anti-myc antibody. Immunoprecipitates were probed for the myc and HA-tagged p150^{Glued} constructs to assess dimerization. Immunoblot (IB) for dynamitin/p50, a subunit of the dynactin complex, and the dynein intermediate chain, DIC, was performed to assess incorporation into the dynein-dynactin complex. GAPDH was probed for as a negative control. Quantification of p150^{Glued} dimerization (C), incorporation into dynactin (D) and association with dynein (E), relative to wild-type. Insets above the graphs illustrate the association tested. Mean ± SEM, n=3–4 independent experiments, $^{**}P$<0.01 compared to wild-type, one-way ANOVA Bonferroni post test. Also see Figures S5 and S6.

NIH-PA Author Manuscript
NIH-PA Author Manuscript
NIH-PA Author Manuscript

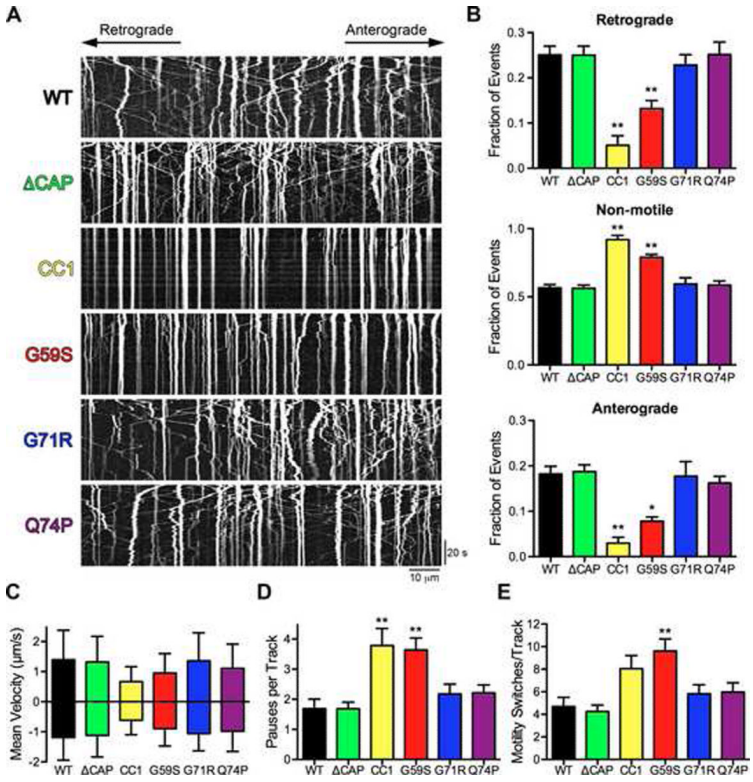

Figure 7. The HMN7B mutation, but not the Perry syndrome mutations, disrupts axonal transport

(A) Kymographs from live-cell time-lapse imaging of LAMP1-RFP in DRG neurons at 2 DIV expressing wild-type (WT), ΔCAP-Gly, CC1, HMN7B (G59S) or Perry syndrome (G71R & Q74P) $p150^{Glued}$. Images were acquired at 366 ms per frame for 2.2 minutes; scale bars for the x and y-axes represent 10 μm and 20 seconds, respectively. Kymographs show the first 180 frames, full movies shown in Movies S4 and S5. (B) Quantification of vesicle motility from the kymographs showed that only the HMN7B (G59S) mutation and CC1 disrupt motility. >575 vesicles were counted per condition. Mean ± SEM, n=5–8 neurons per condition, *P<0.05, **P<0.01 compared to wild-type, one-way ANOVA Bonferroni post test. (C–E) Individual tracks from the kymographs were analyzed. (C) Mean anterograde and retrograde instantaneous velocities ± SD, n>800 instantaneous velocities per condition per direction. Also see Figure S7. Quantification of the number of pauses per track (D) and motility switches per track (E). Mean ± SEM, n>23 vesicles per condition, **P<0.01 compared to wild-type, one-way ANOVA Bonferroni post test.

NIH-PA Author Manuscript
NIH-PA Author Manuscript
NIH-PA Author Manuscript

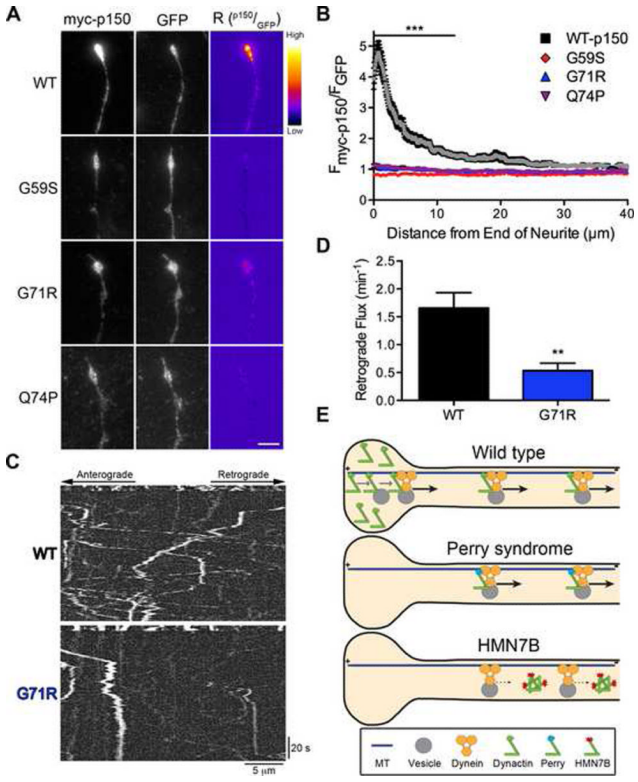

Figure 8. Perry syndrome mutant disrupts flux from the distal neurite

(A) DRG neurons were stained at 2 DIV for myc-tagged wild-type (WT), HMN7B (G59S) or Perry syndrome (G71R & Q74P) p150^{Glued} and GFP, a marker of cytoplasmic volume, expressed from a bicistronic vector. These distal neurite images were individually contrast enhanced to display both axonal and tip staining. The raw myc-p150 data was divided by the corresponding raw GFP signal to create the ratio-image ($R^{p150}/_{GFP}$), which shows the distal accumulation relative to GFP. These ratio-images were contrast enhanced to the same level and a heat map was applied to show the relative intensities of the ratio. The warmer colors represent a higher ratio, while cooler colors represent a lower ratio. Scale bar: 5 μm. (B) Line-scan analysis from the neurite tip. The normalized ratio of myc-p150^{Glued} to GFP fluorescence intensity was determined along the length of the neurite. Wild-type p150^{Glued} accumulated significantly more over the first 14 μm as compared to mutant p150^{Glued}. The WT-p150 data was replotted from Figure 2D. Mean ± SEM, $n \geq 29$ neurite tips from 4–6 neurons per condition, ***$P<0.001$ compared to wild-type, two-way ANOVA Bonferroni post test. (C) DRG neurons expressing wild-type or G71R p150^{Glued} were imaged at 2 DIV. The retrograde flux of LAMP1-RFP from the neurite tip was measured following photobleaching of a zone 10 μm proximal to the end of the neurite. Entry of cargos from the distal tip into this bleach zone was assessed with time-lapse imaging. Images were acquired at 2 frames per second for 5 seconds pre-photobleaching and 120 seconds post-photobleaching. Kymographs of the photobleached zone were made prior to and subsequent to photobleaching to assess the retrograde flux of cargo from the distal neurite. (D) Retrograde vesicle flux was determined by counting the number of retrograde vesicles that moved at least 3.5 μm into the photobleached zone. The Perry syndrome (G71R) mutation dominantly decreased retrograde flux from the distal neurite. Mean ± SEM, n=14–16 neurites from 8 neurons per condition, **$P<0.01$ Student's t-test. (E) Model of how the Perry syndrome and HMN7B mutations differentially disrupt dynactin function. The wild-type model is redrawn from Figure 5C. The Perry syndrome mutations decrease distal dynactin

accumulation and reduce the flux of cargo from the neurite tip. The HMN7B mutation destabilizes dynactin, which decreases the association between dynein and dynactin and disrupts transport throughout the axon.

NIH-PA Author Manuscript
NIH-PA Author Manuscript
NIH-PA Author Manuscript